Available online at www.sciencedirect.com
ScienceDirect
International Journal of Heat and Mass Transfer 51 (2008) 3066–3081
International Journal of HEAT and MASS TRANSFER
www.elsevier.com/locate/ijhmt

Numerical study of film cooled rotor leading edge with tip clearance in 1-1/2 turbine stage

Huitao Yang [a], Hamn-Ching Chen [a], Je-Chin Han [a,*], Hee-Koo Moon [b]

[a] Texas A&M University, College Station, TX 77843, United States
[b] Solar Turbines Incorporated, 2200 Pacific Highway, San Diego, CA 92101, United States

Received 28 September 2006
Available online 14 November 2007

Abstract

Numerical simulations were performed to predict the film cooling effectiveness and the associated heat transfer coefficient in a 1-1/2 turbine stage. The leading edge of the rotor blade is film cooled with three rows of film cooling holes. The rotor tip leakage has been investigated for a clearance of 0.8% of blade span. Sliding grid is used for the rotor domain, and interface technique is employed to exchange information between stator and rotor domains. Simulations were carried out for both design and off-design conditions to investigate the effects of the stator–rotor interaction on the film cooling characteristics. The commercial code FLUENT with Reynolds stress model is used in the prediction. It is found that the tilted stagnation line on the rotor leading edge moves from the pressure side to the suction side, and the instantaneous coolant streamlines shift from the suction side to the pressure side with the increasing rotating speed. For the fixed inlet/outlet pressure ratio of turbine stage, the high rpm reduces the heat transfer coefficient on the rotor due to the low rotor relative velocity, and increases the "sweet spot" on the rotor tip. These trends are well supported by the experimental results.

Keywords: Gas turbine; Film cooling; Rotating blade; Leading edge; CFD

1. Introduction

The inlet temperature of a modern turbine has continually increased to achieve high thrust power and high thermal efficiency. A turbine stage consists of one row of nozzle guide vanes (stators) and one row of rotating blades (rotors). Due to the stagnation flow, the leading edge region of the rotors experiences a high heat load, which may result in material failure because of the high temperature and thermal stress. To reduce the heat load, several advanced internal cooling technologies have been applied in this region, including impingement cooling on the inner wall of the leading edge with different kinds of turbulators, such as pins or ribs, to enhance internal cooling effects. Besides these internal cooling technologies, film cooling, ejecting coolant to the outer surface of the blade, is commonly used in the leading edge region in the real engine. Although the film cooling slightly increases the heat transfer coefficient, the driving temperature difference ($T_{aw} - T_w$) is reduced significantly. Therefore, the overall heat load decreases.

Several experiments have been carried out to study the heat transfer on the leading edge of the rotors in turbine stages. Dunn et al. [1,2] used a full stage rotating turbine of the Garrett TFE 731-2 engine in a shock-tunnel facility and thin-film heat flux gages to study heat transfer on the vane, end walls and rotors. Abhari and Epstein [3] studied the time-resolved heat transfer for cooled and un-cooled rotors by thin heat flux gages. They found that the heat transfer was highly unsteady for rotors in a transonic turbine. Takeishi et al. [4] employed the CO_2 mass transfer analogy technique to measure the local film cooling effectiveness on a rotor blade, and found higher cooling effectiveness on the suction side compared to the pressure side of the blade. They believed that this phenomenon is caused

* Corresponding author.
E-mail address: jc-han@tamu.edu (J.-C. Han).

0017-9310/$ - see front matter © 2007 Elsevier Ltd. All rights reserved.
doi:10.1016/j.ijheatmasstransfer.2007.09.025

Nomenclature

A_c	cross-sectional area of film cooling holes
C_D	discharge coefficient
h	heat transfer coefficient $= q_w/(T_w - T_{aw,0})$ (W/m^2 K)
LE	abbreviation for "leading edge"
M	overall film coolant blowing ratio $(=\rho_c V_c/\rho_\infty V_\infty)$
M_{local}	local blowing ratio $= \rho_{c,local} V_{c,local}/(\rho_{m,local} V_{m,local})$
$\dot{m}_c$	coolant mass flow rate in the coolant plenum (kg/s)
n	number of film cooling holes $= 15$
P	local static pressure (Pa)
PS	abbreviation for "pressure side"
SS	abbreviation for "suction side"
T	temperature (K) or passing time period (s)
Tu	turbulence intensity (%)
U	rotor rotating speed (m/s)
V	absolute inlet velocity of rotor (m/s)
W	relative inlet velocity of rotor (m/s)
y^*	dimensionless distance $(y^* = \rho C_\mu^{1/4} k_p^{1/2} y_p/\mu)$

Greek symbols

η_{aw}	adiabatic film cooling effectiveness $= (T_{aw,0} - T_{aw,f})/(T_{aw,0} - T_{t,c})$
ρ	density (kg/m^3)

Subscripts

0	without film cooling
2	station 2
3	station 3
aw	adiabatic wall
c	coolant
f	with film cooling
m	mainstream
t	total or stagnation value
p	near wall cell
w	wall of blade
∞	turbine stage inlet

by the effect of the radial flow and strong mixing on the pressure surface. Camci and Arts [5,6] made high pressure rotor blade heat transfer measurements in a short duration wind tunnel facility. They found that the cooling efficiency increases with decreasing T_c/T_{in} (i.e., coolant temperature/inlet gas temperature). Mehendale et al. [7,8] studied the effect of high free stream turbulence and upstream wake on heat transfer and film cooling of a rotor blade in a low speed wind tunnel facility. They concluded that the high turbulence and wake increases the heat transfer slightly, but significantly reduces the film cooling effectiveness for lower blowing ratio conditions. Du et al. [9] used the same facility to study the effect of a simulated unsteady wake on the detailed Nusselt number and film cooling effectiveness distribution of a rotor blade by the transient liquid crystal technique. Rhee and Cho [10,11] have employed the naphthalene technique to study the heat/mass transfer on the rotating blade, found the high rpm reduces the heat transfer on the rotor tip with the changing incident angle of rotor relative velocity. Recently, Ahn et al. [12] used a pressure sensitive paint (PSP) technique to study the detailed distribution of film cooling effectiveness on the leading edge of the first-stage rotor blade in a three-stage turbine. They concluded that the film cooling protection shifts from the suction side to the pressure side with increasing rotating speed, and the film cooling effectiveness slightly enhances with increasing blowing ratio in the range they studied.

Numerical predictions of heat transfer and film cooling on rotor blades have been performed by many researchers. Abhari et al. [13] examined the time-resolved aerodynamics and heat transfer in a transonic turbine rotor. They concluded that there is relatively little difference between the steady state turbulent and the time averaged unsteady calculations. In general, the measured Nusselt number is either higher than or equal to the predicted Nusselt number. Dunn et al. [14] reported the time-averaged Stanton number and the surface pressure distribution for the first-stage vane row and the first-stage blade row. They found that the heat transfer shows small differences of prediction among different turbulence models. Ameri and Steinthorsson [15] used a multi-block code, TRAF3D, to calculate the Stanton number of a rotor, and the results at the 90% span location of blade are in good agreement with the experimental data. Zhang and Ligrani [16] used FLUENT code with k–ε RNG turbulence closure model to study the skin friction factor, Stanton number and aerodynamics losses for a turbine vane. Their prediction showed that the skin friction factor and Stanton number increase with increasing surface roughness and turbulence intensity, or decreasing Mach number. Leading edge film cooling with compound angle holes was numerically studied by Lin et al. [17] using CFL3D code. Compared to the experimental data, the numerical prediction shows a good agreement in the trend of the adiabatic film cooling effectiveness, but the value is over-predicted. Garg and Ameri [18] used q–ω, k–ε and k–ω turbulence models to predict the heat transfer on a film cooled airfoil. Overall, the q–ω model and the k–ε model predict similar results, while the k–ω model predicts higher heat transfer coefficients. Yang

et al. [19,20] compared various turbulence models on the prediction of heat transfer on GE-E^3 plane tip and squealer blade tips, and found that there is small difference among the different turbulence models on the plain blade tips, and little improvement by the Reynolds Stress Model for the squealer tip. Yang et al. [21] studied the blade tip film cooling with three different film hole arrangements on plane and squealer tips by numerical methods, and demonstrated that the upstream and two-row film hole arrangements provided higher overall film cooling effectiveness compared to the camber line arrangement. They also found a good agreement with experiment in the heat transfer coefficient, but the magnitude of film cooling effectiveness was over-predicted. Recently, Yang et al. [22] have performed a numerical study of two-row film cooling on the leading edge of a rotor blade in a 1-1/2 turbine stage. They concluded that the film cooling and heat transfer show an unsteady character due to the interaction of a rotating blade in a turbine stage.

Until now, very few researches were reported in the open literature to study the effect of stator–rotor interaction on the detailed film cooling effectiveness and the associated heat transfer coefficient of the rotor blade in a complete turbine stage. In the present study, numerical simulations were performed to investigate the effect of different working conditions on the three-row film cooled rotor blade in a 1-1/2 turbine stage with tip clearance, which is similar to the turbine stage experimentally studied by Ahn et al. [23] using the Pressure Sensitive Paint (PSP) measurement technique.

2. Computational details

The present unsteady three-dimensional calculations were carried out for a 1-1/2 turbine stage, which includes the first-stage stator (stator 1), the first-stage rotor (rotor), and the second-stage stator (stator 2), as shown in Fig. 1. Only the leading edge of rotor blade is film cooled in the present study. The blade height is 63 mm, the root of blade diameter is 558.8 mm, and the shroud diameter is 685.8 mm. The rotor blade tip clearance is 0.504 mm, corresponding to 0.8% of the rotor span. Both the stator and rotor blades are two-dimensional with the same blade profiles in the spanwise direction, which is exactly the same as the experimental blade used by Ahn et al. [23]. In their experiment, there are 58 blades in first-stage stator, 46 blades in first-stage rotor, and 52 blades in second-stage stator. To simulate the experimental conditions exactly, it is desirable to use 29 first-stage stator blades, 23 rotor blades, and 26 second-stage stator blades with periodic

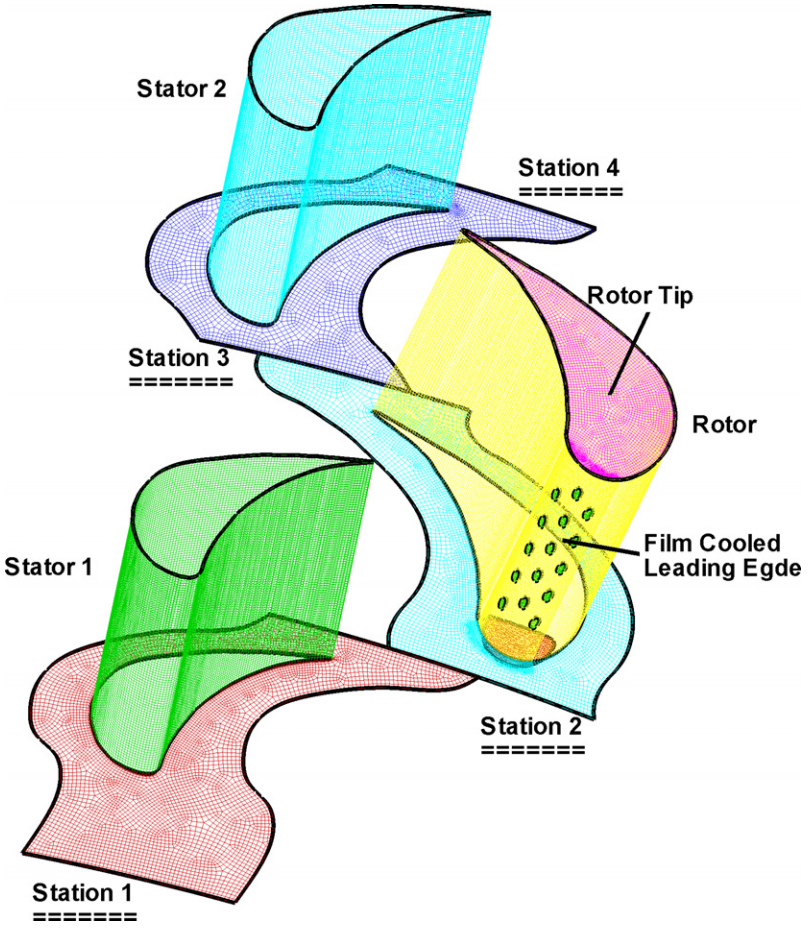

Fig. 1. Computational domain and numerical grids for 1-1/2 turbine stage.

boundary conditions in the circumferential direction. In order to significantly reduce the CPU time and computer memory requirements, it is necessary to use the same number of blades for both the rotor and stators in the 1-1/2 turbine stage. This enables us to simulate only one flow passage with periodic boundary conditions in the circumferential direction. Since the present study focuses on the leading edge film cooling of the rotor blade, it is reasonable to simplify the turbine stage by using 46 blades for both the first- and second-stage stators while maintaining the correct number of rotor blades. For the film cooled rotor blade, there are 15 film cooling holes in the leading edge region arranged in three rows: pressure side row, leading edge row, and suction side row. Each row has five film cooling holes with a hole diameter of 1.19 mm. The spanwise spacing of the film cooling holes is 9.5 mm, which gives a pitch-to-diameter ratio of 7.95. The pressure and suction side rows are located at $\pm 23.58°$ from the leading edge. The film cooling holes are oriented to the spanwise (radial) direction and inclined to the blade surface by 30°. The film cooled rotor blade is exactly the same as that used in the experiment. More detailed geometries of the stator and the film cooled rotor blades are given in Ahn et al. [23]. Other information of that research turbine rig with two-dimensional blades can be found in Schobeiri et al. [24,25]. Calculations were performed with three different rotating speeds: 2100, 2550, and 3000 rpm, corresponding to the low rpm, design rpm, and high rpm conditions, respectively. It should be remarked that the low rpm condition tested by Ahn et al. [23] was 2400 rpm, but a wider range of rotating speeds is considered in the present numerical simulations to facilitate a better understanding on the effects of rotation. The inlet total and exit static pressures of the turbine stage are $P_{t,in} = 101{,}356$ Pa and $P_{ex} = 85{,}000$ Pa, resulting in a pressure ratio ($P_{t,in}/P_{ex}$) of 1.19. The total temperature (325 K) and turbulence intensity (5%) are specified at turbine stage inlet with an inlet flow angle of 0°.

The simulations were performed using the CFD software package FLUENT (version 6.2) [26]. The solutions are obtained by solving the compressible Reynolds-Averaged Navier–Stokes (RANS) equations using a finite volume method to discretize the continuity, momentum and energy equations. The GAMBIT software was used to generate the unstructured grids, with a fine grid clustering around the blade boundary layer. The computational domain consists of fluid around the first-stage stator blade, a film cooled rotor blade with tip clearance, and the second stage stator blade. The periodic boundary condition has been imposed in the circumferential direction for both stators and rotor as shown in Fig. 1. The computational domain is divided into two regions with different grid structures to ensure adequate resolution of the complex three-dimensional flow and heat transfer in the film cooled leading edge of the rotor blade. The domain of the 1-1/2 turbine stage is composed entirely of the hexahedral cells, which are more accurate with less numerical diffusion. The second domain consists of three rows of film-hole tubes connected with a semi-circular plenum. Tetrahedral cells are used in the film coolant domain since they are flexible to construct. An interface technique was employed to handle the two different types of grids and the stator/rotor domain. Relatively coarse grids are used for the majority of the 1-1/2 turbine stage. To achieve accurate resolution of the film cooling effectiveness and heat transfer, much finer grids are applied to the film-holes tubes, the rotor leading edge, tip clearance of the rotor and near wall regions of the blades. In the leading edge region of the rotor and the boundary layers of the stator and rotor blades, the y^* value for the near wall grids falls between 30 and 100. The rotor tip, however, has a small value of y^* because of the narrow clearance. Therefore, the enhanced wall treatment has been applied to handle these complicated boundary conditions. The principle of the enhanced wall treatment is that it combined the non-equilibrium wall function with two-layer model in the near wall region. When y^* is a small value, the two layer model is applied, otherwise the non-equilibrium wall function will be employed to handle a large y^*. The geometry and detailed grid distribution of a typical film tubes on the rotor leading edge are shown in Fig. 2.

The inlet velocity of the turbine stage is 30 m/s. Depending on the overall blowing ratio, a constant mass flux boundary condition is specified at the inlet of the coolant plenum, and the coolant temperature is equal to 300 K. Three sets of calculations with different thermal boundary conditions were performed to achieve the adiabatic film cooling effectiveness $\eta_{aw} = (T_{aw,0} - T_{aw,f})/(T_{aw,0} - T_{t,c})$, and the heat transfer coefficient $h = q_w/(T_w - T_{aw,0})$. For the calculation of $T_{aw,f}$, the turbine inlet total temperature is specified at $T_{t,\infty} = 325$ K and the coolant total temperature is $T_{t,c} = 300$ K. The adiabatic wall boundary condition is used for the blades wall to obtain $T_{aw,f}$. It should be noted that $T_{aw,f}$ includes not only the effects of film cooling, but also the temperature changes due to the turbine work process. In order to determine the pure film cooling effectiveness η_{aw} without the complication caused by the turbine work process, it is desirable to calculate another adiabatic wall temperature $T_{aw,0}$ for the same flow condition in the absence of film coolant injection. This enables us to determine the true effect of coolant protection by comparing the temperature differences between the two cases (with and without the presence of film coolant). For the simulation of heat transfer coefficient, the coolant total temperature is kept the same as the turbine inlet total temperature 325 K, while the wall temperature is fixed at 300 K to calculate the wall heat flux q_w. The heat transfer coefficient is calculated from $h = q_w/(T_w - T_{aw,0})$. This definition of heat transfer coefficient depends only on the passage flow condition, and will not be affected by the turbine work process which was discussed in details in Yang et al. [27].

All calculations are converged to residual levels of the order of 10^{-5}, and to less than 0.1% error in the mass flow rate between the main stream and coolant inlet and outlet

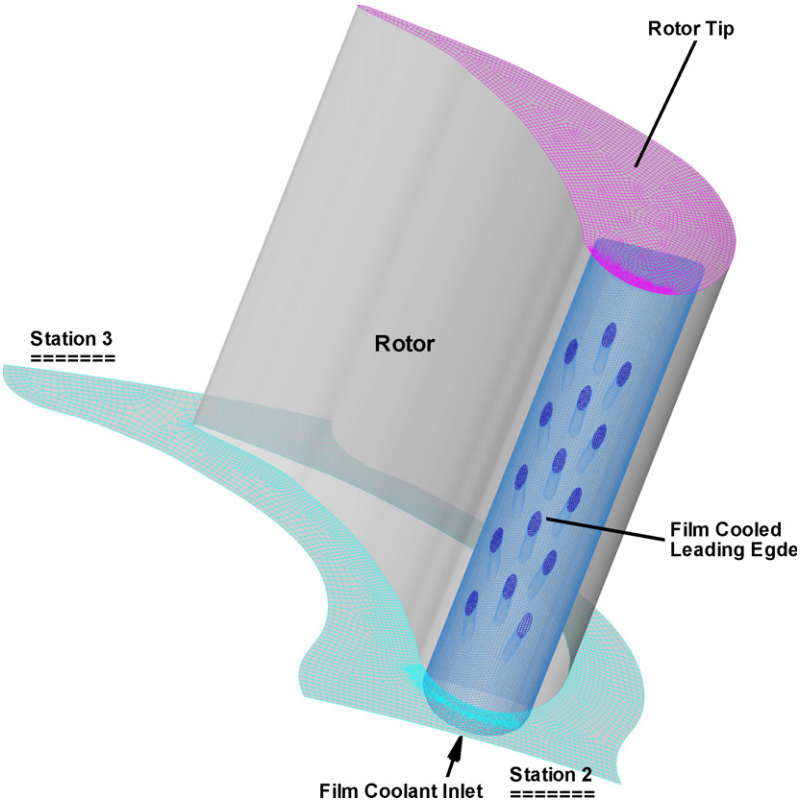

Fig. 2. Film cooled leading edge of a rotor blade and grid structure for film cooling holes.

of the computational domain. The selection of the time step is critical for accurate time-dependent flow predictions. Here, 100 time steps are used in calculating one passing period of the rotor blade. The passing period, T, is defined as the time it takes for the rotor blade to move from one stator row to another. The computed results are recorded and analyzed every 25 time steps (i.e., every 1/4 passing period). To achieve good periodic results, simulations were performed for 10 passing periods and the numerical results are presented at four different time phases with $t/T = 91/4$, 91/2, 93/4, and 10, respectively. The grid refinement study has been carried out with two sets of

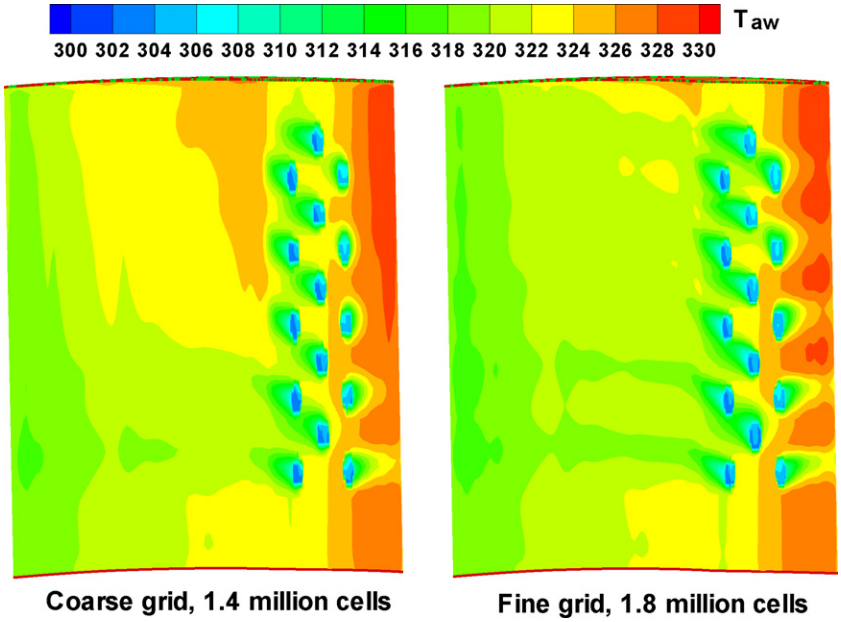

Fig. 3. Grid refinement study.

grids. The stator 1 and stator 2 computational domains consist of 0.4 million cells respectively, and do not change since this study mainly focus on the film cooled rotor. For the coarse grid case, the rotor domain has about 0.6 million cells. For the fine grid, the number of grid points in rotor domain was increased to about 1 million cells. Note that the near wall grid distance stays the same for these two sets of grids to keep the y^* values between 30 and 100. Fig. 3 shows a comparison of the dimensionless temperature distributions for the coarse and fine grid cases. The difference between these two grids is small on the rotor leading edge, thus the fine grid solution is nearly grid independent. All the numerical results presented here were obtained using the fine grid. Since these simulations involve unsteady three-dimensional flow with a sliding mesh technique, they are computationally intensive. Each case takes about two weeks of CPU time on the SGI Altix 3700 supercomputer at Texas A&M University. Due to the limitation in available computing resource, the present investigation focuses on the overall effect of film cooling on the rotor in a 1-1/2 turbine stage instead of detailed film coolant behavior near the film holes.

3. Flow structure study

Simulations are performed at three overall blowing ratios (M) of 0.5, 1.0, and 2.0 with density ratio 1.0. The overall blowing ratio is defined as $M = \rho_c V_c / \rho_\infty V_\infty$. The density ratio is unity in the current study; therefore the mass flux ratio is reduced to velocity ratio. V_∞ is the mainstream velocity, relative to the rotor blade, at the inlet of the rotor blade. Based on the above definition, the coolant mass flow rate required by the coolant plenum ($\dot{m}_c$) for a given overall blowing ratio was pre-determined by Eq. (1), and specified at the inlet of the plenum.

$$\dot{m}_c = n \cdot M \rho_m V_m A_c \tag{1}$$

The coolant mass flow rate is not evenly distributed among the holes due to the varying pressure differential across the holes. Hence, the actual or local blowing ratio, defined as $M_{local} = \rho_c V_{c,local} / \rho_m V_{m,local}$, is examined for each hole. $V_{m,local}$ is the local velocity of the oncoming mainstream, relative to the rotor, near the film cooling holes and $V_{c,local}$ is the averaged actual coolant velocity from the film cooling hole. $V_{m,local}$ is determined by the pressure distribution on the blade surface (total pressure P_t and static pressure P) and the velocity triangle. To obtain the actual coolant mass flow rate from each hole, the discharge coefficients C_D is calculated by

$$\dot{m}_c = \sum_{i=1}^{n} C_D \cdot A_c \cdot \sqrt{2(P_{t,plenum} - P)/\rho_c} \tag{2}$$

The discharge coefficient C_D is assumed to be constant for all holes in the cavity for a given overall blowing ratio M. It should be noted that the constant assumption of C_D may not be true as C_D depends on not only the geometry but also the external and internal flow conditions. It is assumed that the deviation in the discharge coefficients from hole to hole is not significant and hence an average value can be used without introducing a significant error. Once the C_D for a given M is determined, the coolant velocity from each hole is calculated by

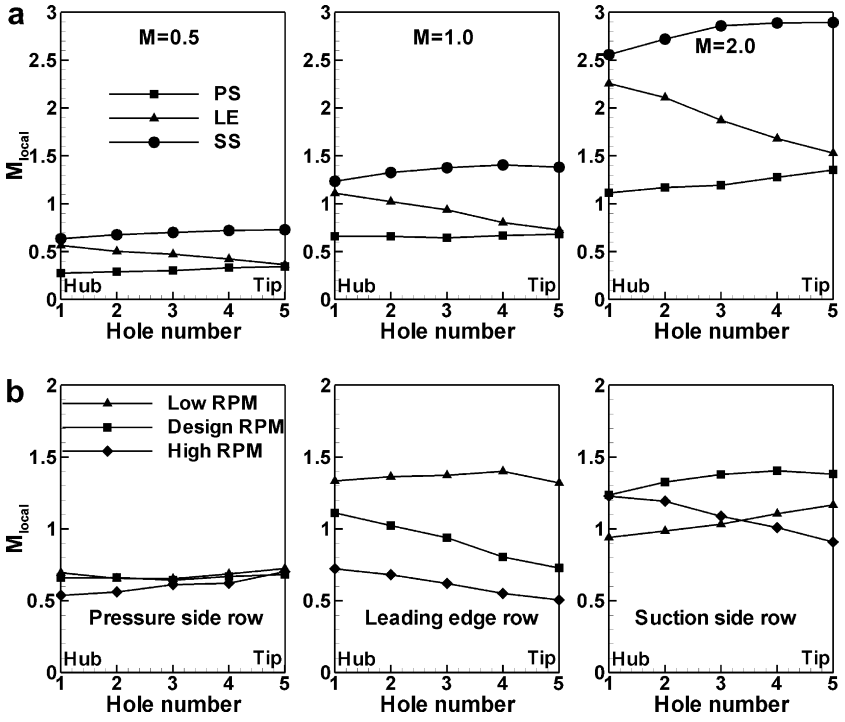

Fig. 4. Local blowing ratio distribution: (a) at design RPM, (b) at different RPM with $M = 1$.

$$V_{c,local} = C_D \cdot \sqrt{2(P_{t,plenum} - P)/\rho_c} \quad (3)$$

Having obtained $V_{c,local}$ and $V_{m,local}$, the actual (or local) blowing ratio for a particular hole is computed based on the local blowing ratio definition. Fig. 4a shows the local blowing ratio distribution at design rotating speed. Although the mainstream velocity near the suction side row is slightly higher than that near the other two rows, the low pressure on the suction side results in much more coolant ejection to the suction side. Consequently, for a given overall blowing ratio, the local blowing ratio on the suction side is significantly higher than those on the pressure side and leading edge. The local blowing ratio variation in the spanwise direction is relatively small except on the leading edge row at $M = 2$. Fig. 4b shows the local blowing ratio distribution for $M = 1.0$ at different rotating speeds. The local blowing ratio distribution on the pressure side does not vary much with the rotating speed. Larger variation takes place on the leading edge with highest blowing ratio at low rpm. At $M = 1$, the local blowing ratio distribution in the spanwise direction is relatively uniform for all the rotating speed.

Fig. 5 compares the instantaneous streamlines and Mach number contours at the mid-span plane of the turbine stage based on the absolute as well as relative reference frames for three rotating speeds. For the earth-fixed absolute reference frame, the streamlines follow the stator 1 passage and push against the rotor as shown in Fig. 5a. Therefore, the rotor rotates and transfers a portion of the gas total energy to mechanical energy. It is worthwhile to note that the rotor absolute inlet velocity does not change significantly for various rotating speeds, because it mainly depends on turbine stage inlet/outlet pressure ratio which was kept constant for all three different rotating speeds. Fig. 5b shows the streamlines based on the relative velocities on a rotor-fixed reference frame. The three arrows with solid lines denote the incident angle of rotor relative inlet velocity for the design rpm condition, while the arrows with dashed line indicate the instantaneous incident flow directions for the off-design conditions. In general, the incident flow angle changes with rotating speed but the streamlines align smoothly with the rotor blade surface in all cases. For the low rpm case, the relative velocity impinges on the leading edge pressure side with a positive incident angle. At the design condition, the flow leaving the first-stage stator impinges directly on the leading edge of the rotor blade with zero incident angle. For the high rpm case, the relative velocity impinges on the leading edge suction side with a negative angle of attack. The change of the rotor relative velocity incident angle significantly impacts on the direction of film cooling protection on the leading edge, which will be discussed further in the later section.

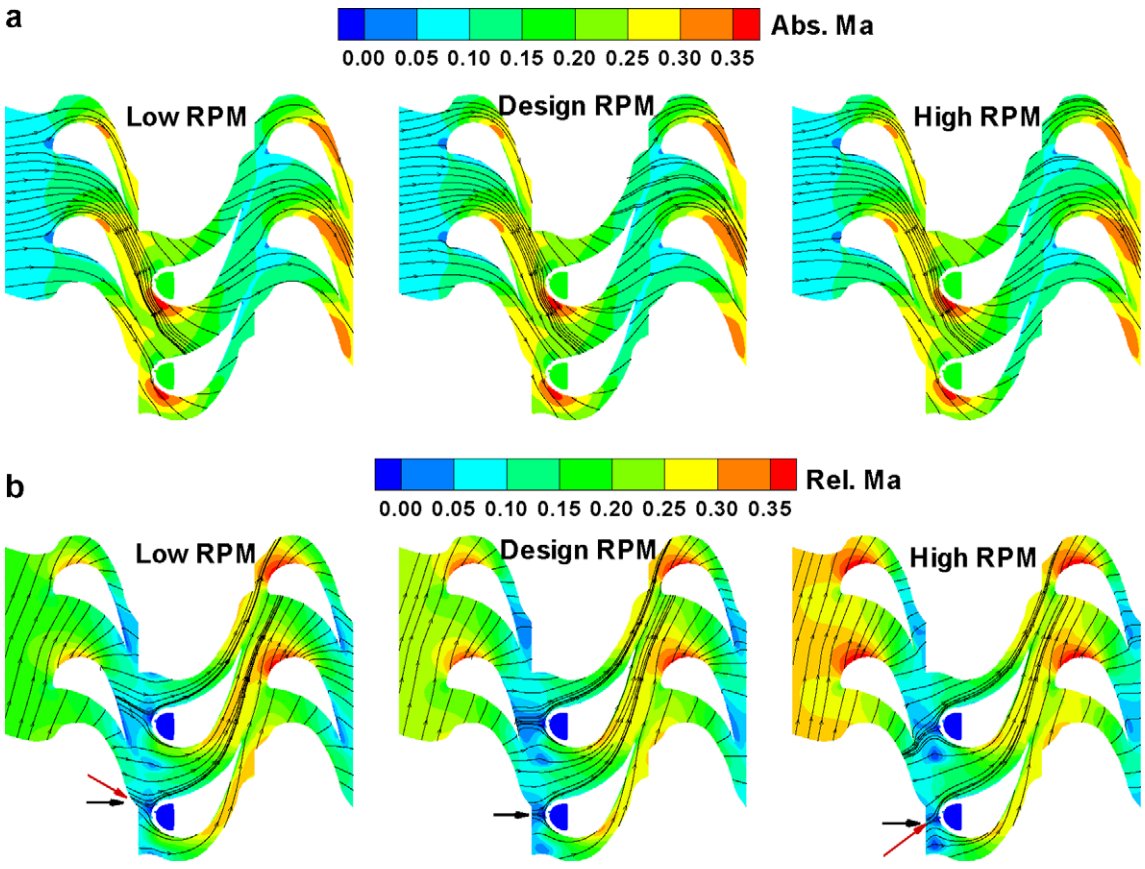

Fig. 5. Velocity field at mid-span plane with Mach number contours at time phase 1/4: (a) instantaneous streamlines based on the absolute reference, (b) instantaneous streamlines based on the relative reference.

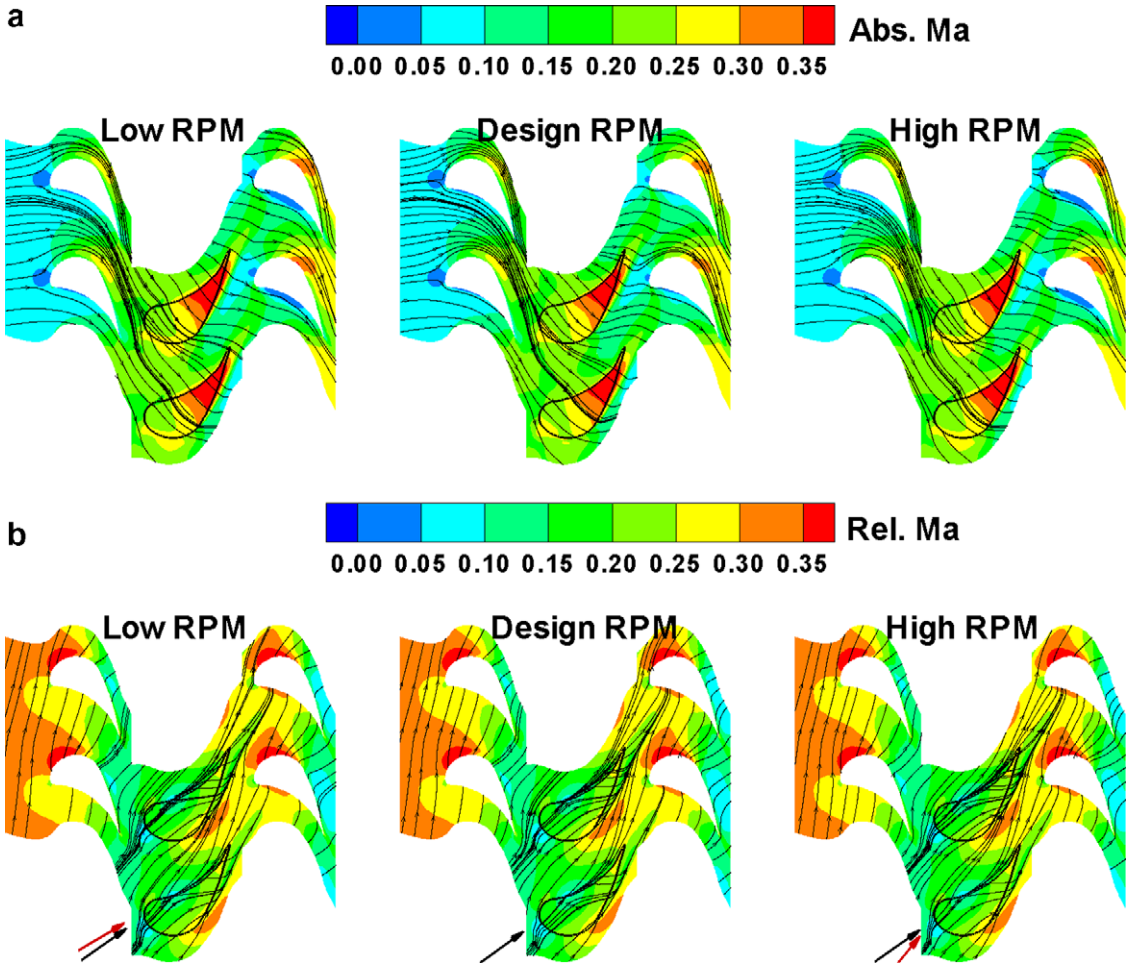

Fig. 6. Velocity field at mid-gap plane with Mach number contours at time phase 1/4: (a) instantaneous streamlines based on the absolute reference, (b) instantaneous streamlines based on the relative reference.

Fig. 6a and b show the instantaneous streamlines at mid-gap plane in the fixed (i.e., absolute velocity) and rotating (i.e., relative velocity) reference frames, respectively, for three rotating speeds. The mid-gap plane is a constant-radius surface located at the middle of the rotor tip and the shroud. It is seen from Fig. 6a that the streamlines in absolute reference frame are guided by the stators and move across the rotor blade tip gap to the blade suction side. The general flow directions on the pressure side of the blade tip is similar to those observed on the mid-span plane shown earlier in Fig. 5a. On the other hand, the streamlines on the blade suction side turn sharply near the trailing edge due to the presence of tip leakage flow. The detailed tip leakage flow pattern can be more clearly visualized in the rotating reference frame. In Fig. 6b, the arrows with solid lines denote the incident angle of rotor relative inlet velocity at the design condition while the arrows with dashed lines denote the incident flow angle for off-design conditions. For all three rotating speeds, the tip leakage flow was driven by the blade pressure gradient from the pressure side to suction side. Comparing to the mid-span flow patterns shown earlier in Fig. 5b, it is clearly seen that the tip leakage flow has led to a sharp shift of the incident flow direction toward the blade suction side for both the design and off-design conditions. On the blade suction side, the streamlines across the blade tip gap converge into a limiting streamline to form a tip leakage vortex in the trailing portion of the blade tip. The leakage flow pattern in the blade trailing portion is only slightly affected by the rotating speed since it is controlled primarily by the blade pressure gradient. Around the blade leading edge region, however, the incident flow angle is strongly affected by the rotating speed.

Fig. 7 shows the instantaneous streamlines on the rotor outlet plane at four time phases for the design condition. Both the streamlines on the inlet and outlet planes of the rotor were plotted in the fixed reference frame using the absolute velocity. On the rotor inlet plane, the streamlines move smoothly from pressure side to suction side without much distortion. On the other hand, the streamlines on the rotor outlet plane is strongly affected by the rotor blade tip vortex with complex secondary flow patterns which vary significantly at four different time phases. At time phase 1/4, there are two vortices behind the rotor blade

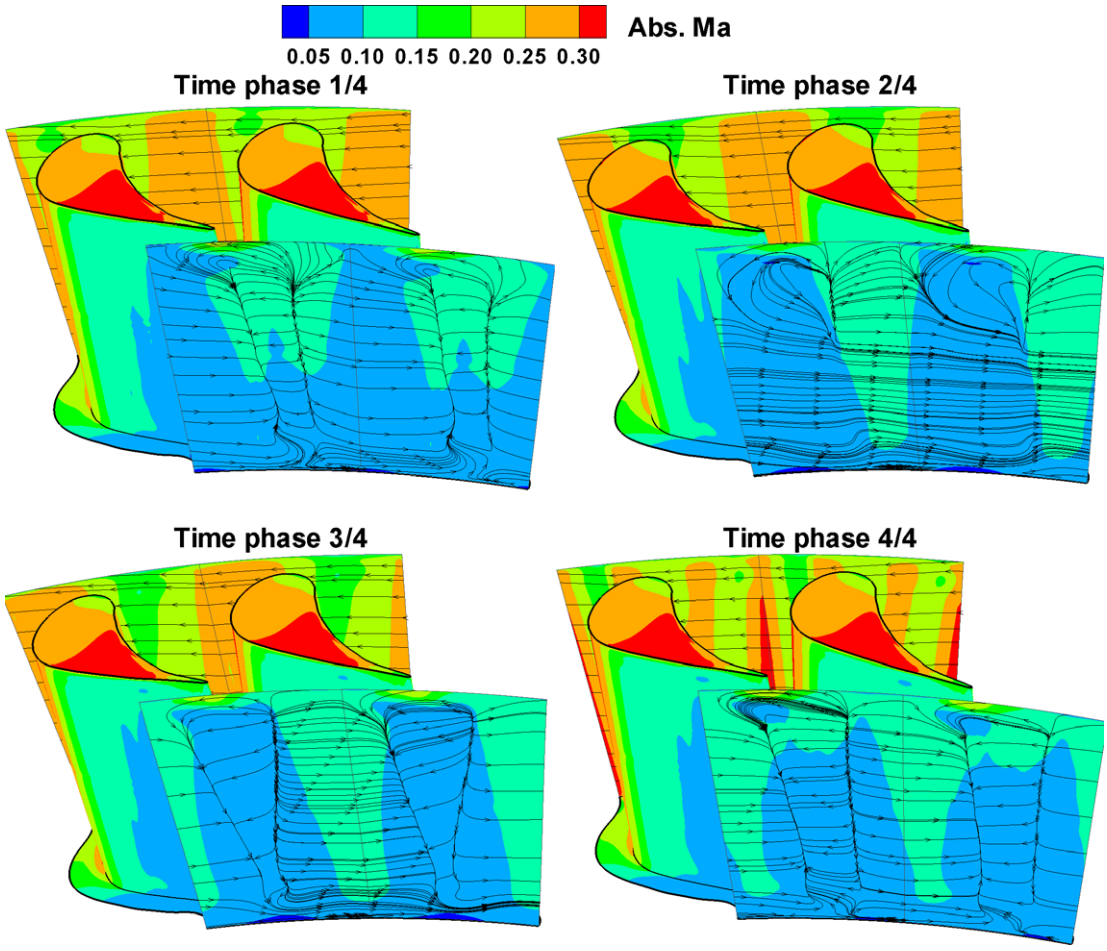

Fig. 7. Instantaneous streamlines on the rotor outlet plane based on the absolute reference for four time phases at design rpm and $M = 1$.

trailing edge. The stronger vortex in the blade tip region is caused by the leakage flow through the tip clearance, while the wake extending from the blade hub to tip is the passage vortex. When the rotor moves to time phase 2/4, the rotor wake flow is the strongest among the four time phases and completely overpowers the passage vortex. The blade tip vortex is also weakened by the rotor wake flow but becomes more visible in the absence of the passage vortex. At time phase 3/4, the passage vortex reappears and merges with the tip leakage vortex into a single vortex extending from the blade hub to the tip. The passage and blade tip vortices continue to strengthen through time phase 4/4 and become two distinct vortices at time phase 1/4 of the next cycle. It is also worthwhile to note that there is a weak secondary flow near the hub region of the rotor outlet plane. However, this secondary flow is considerably weaker than the tip leakage vortex.

Fig. 8 shows the instantaneous coolant streamlines (colored by the adiabatic wall temperature) for four time phases at the design rpm with overall blowing ratio $M = 1$. As expected, the coolant jets are split on the rotor blade pressure and suction sides under the design condition. The coolant from top holes of leading side row shifts to the pressure side due to the tilted stagnation line on this two-dimensional blade. More detailed discussions regarding the tilted stagnation line were given in our previous study for the same 1-1/2 turbine stage [22,27]. It is also interesting to note that some coolant flows over the blade tip clearance due to the tip leakage flow. The coolant from pressure side row and leading row near the blade tip region were driven by the pressure gradients across the trailing section of the rotor blade tip gap. A portion of coolant from the top region of suction side row also flows over the rotor tip leading portion and form a leakage vortex on the rotor blade suction side. It should be noted that the coolant streamlines exhibit unsteady characteristics during these four time phases, especially on the blade tip.

Fig. 9 compares the instantaneous coolant streamlines (colored by the adiabatic wall temperature) for at time phase 1/4 for various rotating speeds. Our previous study [22] showed that the tilted stagnation line (the solid line on the rotor leading edge) moves from the pressure side to the leading edge, and then to the suction side with increasing rpm. For the low rpm condition, the tilted stagnation line lies on the pressure side of the rotor blade. Consequently, most of the coolant from the leading edge row shifts to the suction side while some coolant of the top region leading edge row still cover the pressure side. For

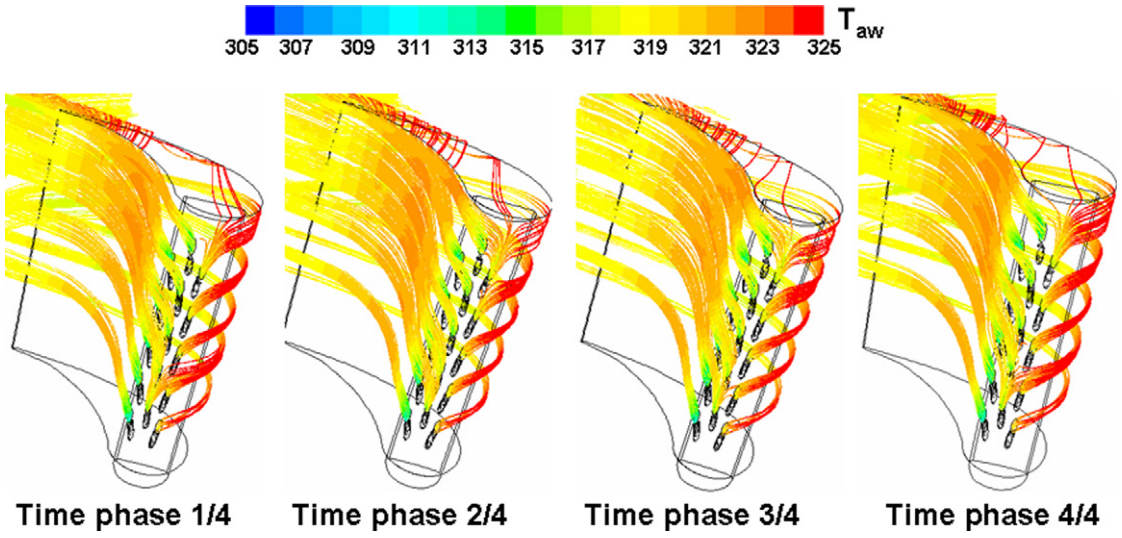

Fig. 8. Coolant pathlines (colored by the adiabatic wall temperature) for four time phases at design rpm and $M = 1$.

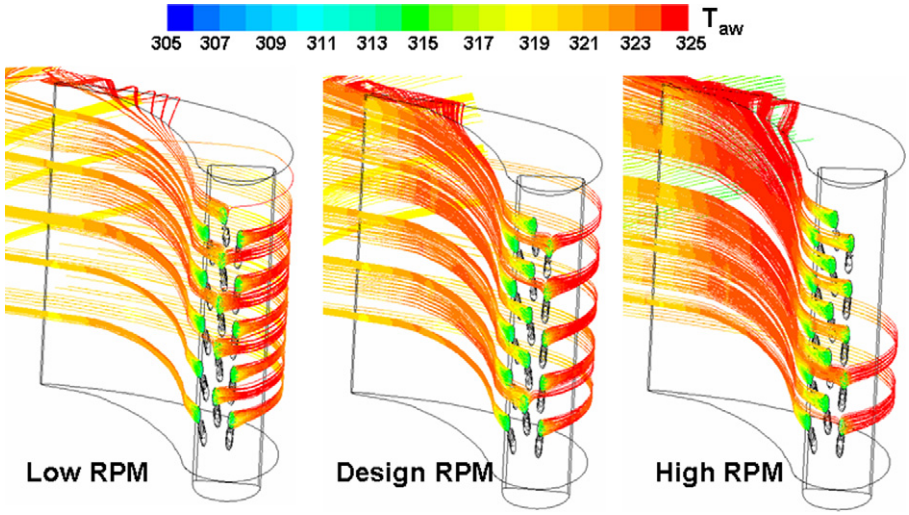

Fig. 9. Comparison of coolant pathlines (colored by adiabatic wall temperature) and conceptual tilted stagnation lines (black solid line) for various rotating speeds at time phase 1/4 and $M = 1$.

the design condition, as expected, the coolant splits evenly on both pressure and suction sides, respectively. However, the coolant from the top region of leading edge row is shifted to the pressure side while the coolant from the bottom region of leading edge row goes to the suction side because of the tilted stagnation line. For the high rpm condition, the stagnation line moves to the suction side and most coolant jets are pushed to the pressure side with very little coolant protection left on the suction side of the blade. Due to the tilting of stagnation line, the coolant from the bottom two suction holes remains on the suction side and provides some protection in the hub region of the suction side. It is worthwhile to note that the coolant tip leakage flow also shows significant difference under different rotating speeds. For the low rpm case, only a small amount of the coolant goes over the blade tip because most coolants were pushed to the suction side. As the rotating speed increases, more coolants were shifted to the pressure side and mixed with the tip leakage flow to improve the protection of blade tip region.

4. Heat transfer study

Fig. 10 compares the heat transfer coefficient for various rotating speeds at time phase 1/4 and $M = 1$. Using the rotor velocity triangles given in our previous study [22], it was quite clear that the relative velocity of the rotor blade decreases with increasing rotating speed. This is responsible for the reduction of the heat transfer coefficient on the rotor blade under high rpm conditions as shown in Fig. 10. In general, the coolant jets disturb the mainstream flow and increase the heat transfer downstream the film holes. The enhancement of heat transfer by the coolant jets is more pronounced on the pressure side where the overall

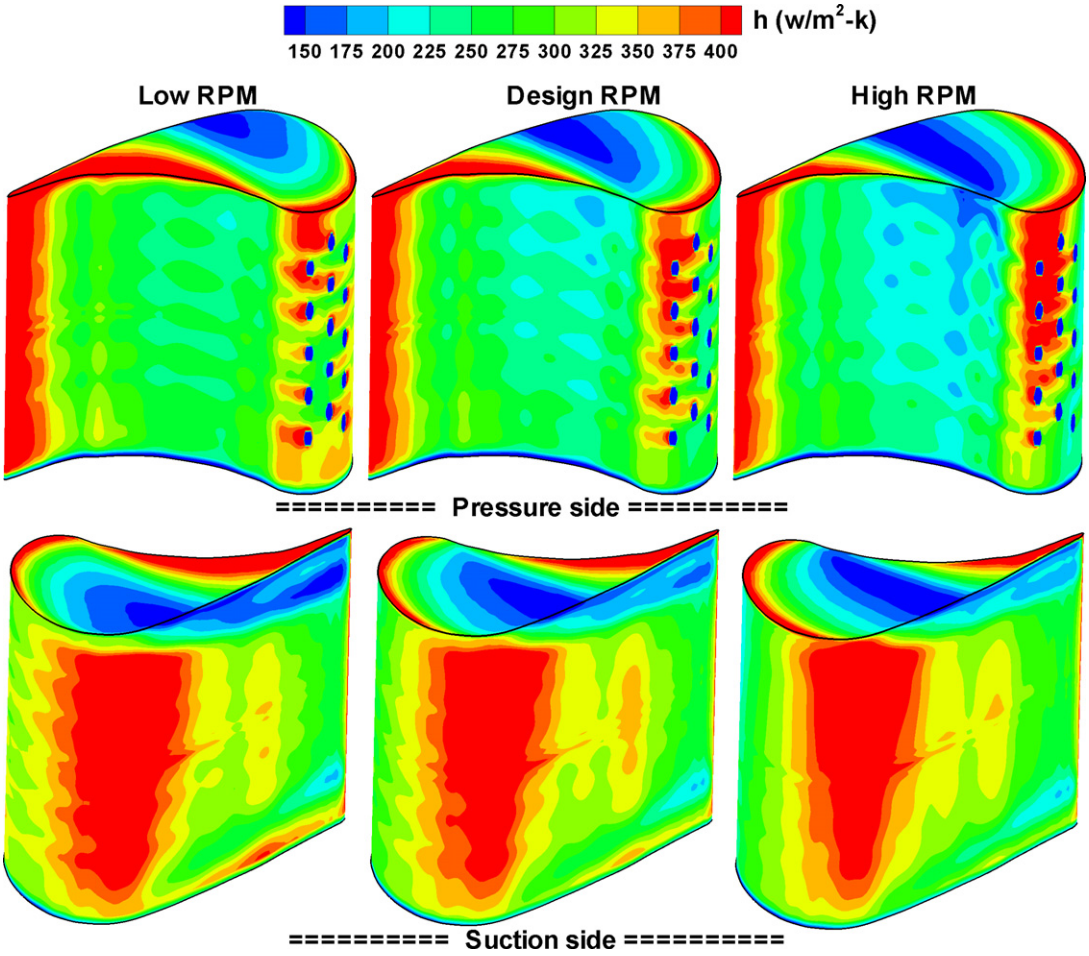

Fig. 10. Heat transfer coefficient distributions on rotor blade for various rotating speeds at time phase 1/4 and $M = 1$.

heat transfer coefficient is lower. On the other hand, the secondary flow induced by the end walls tends to reduce the heat transfer coefficients around the blade tip and hub regions. It is also worthwhile to note that the high rotating speed significantly reduces the rotor secondary flow because of the low relative velocity and negative incident angle. For the low rpm case, the rotor is subjected to a high relative velocity with relatively high heat transfer coefficients. The stagnation line lies on the pressure side and the coolant jets shift to the suction side to increase the heat transfer coefficient on the blade suction side. At the design rpm, the rotor relative velocity decreases which leads to a

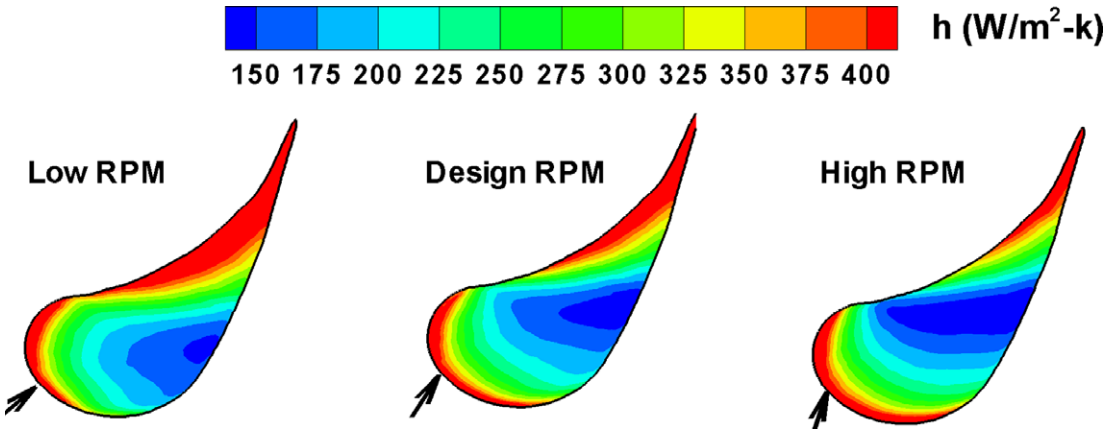

Fig. 11. Comparison of heat transfer coefficients and tip leak velocity angles on the rotor blade tip for various rotating speeds at time phase 1/4 and $M = 1$.

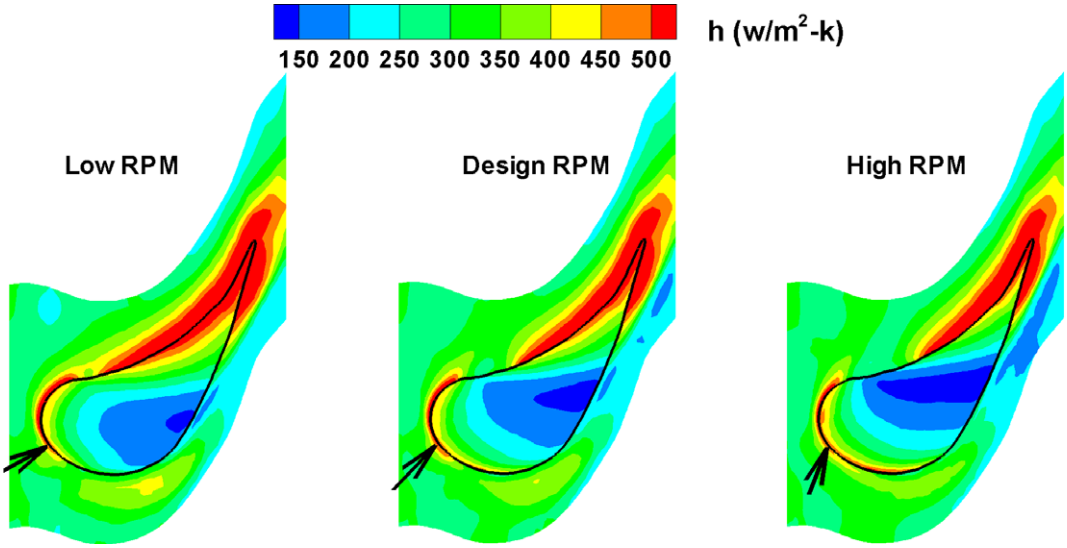

Fig. 12. Comparison of heat transfer coefficients and tip leakage velocity angles on the shroud for various rotating speeds at time phase 1/4 and $M = 1$.

reduction of heat transfer coefficient in comparison with the low rpm case. The tilted stagnation line moves to the leading edge and the coolant jets split evenly between the pressure and suction sides of the rotor blade. For the high rpm condition, the rotor has the lowest heat transfer coefficient since the relative inflow velocity is significantly lower than the other two cases. However, the heat transfer coefficient is high on the pressure side of the leading edge since

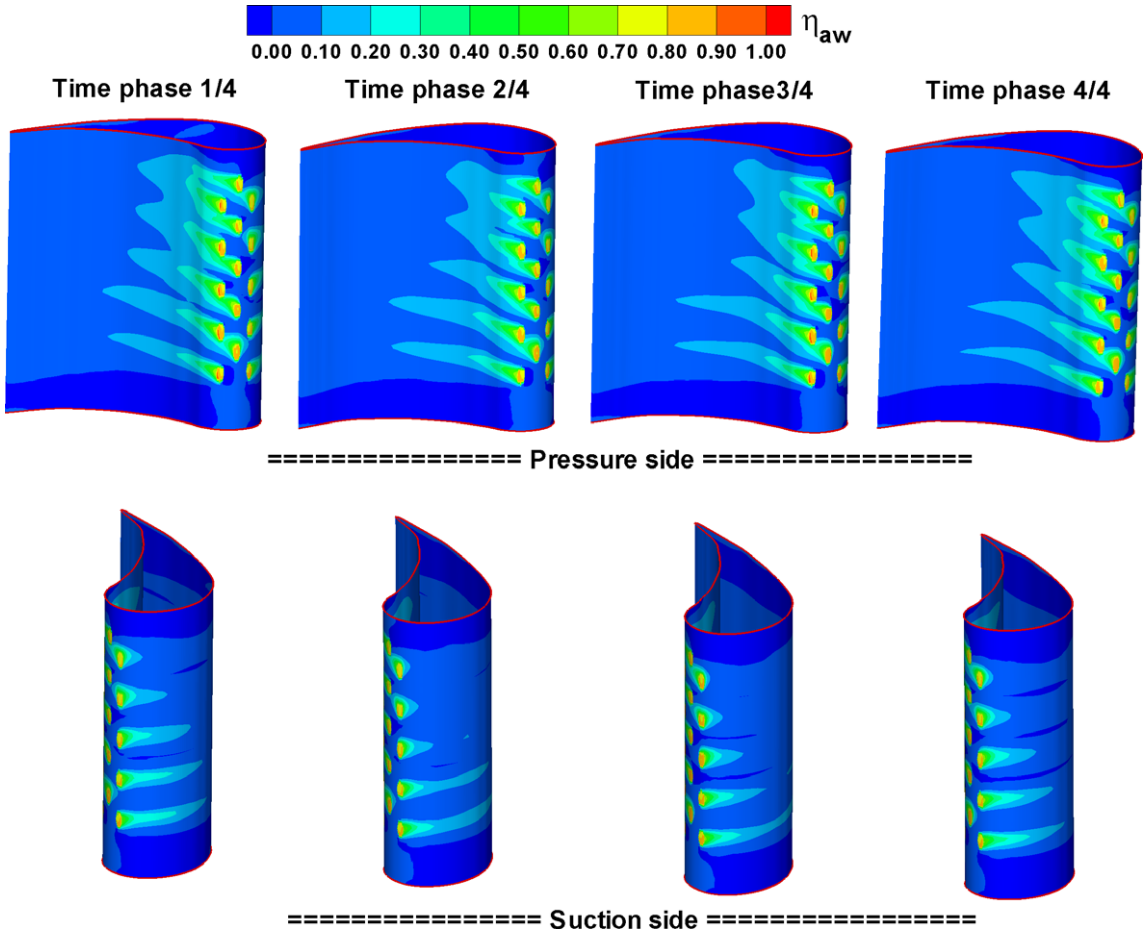

Fig. 13. Adiabatic film cooling effectiveness distributions for various time phases at design rpm and $M = 1$.

most coolant jets were shifted to the pressure side under high rpm condition as shown earlier in Fig. 9. The trend that the high rotating speed reduces the overall heat transfer coefficient on the rotor blade was well supported by the experimental studies of Rhee and Cho [10,11].

Fig. 11 shows a comparison of the heat transfer coefficients on the rotor blade tip for various rotating speeds. For completeness, the relative inlet velocity incident angles are also plotted to facilitate a more detailed understanding of the blade tip heat transfer characteristics. As shown earlier in Figs. 5 and 6, the relative incident angle for the tip leakage flow is drastically different from that at the mid-span plane. Under the high rpm condition, the heat transfer coefficient on the blade tip is reduced since the rotor relative velocity decreases with increasing rotating speed. There is a "sweet spot" with low heat transfer coefficient on the rotor blade tip. With increasing rotating speed, the sweet spot expands significantly and shifts towards the trailing edge. For the low rpm case, the rotor tip leakage flow enters into tip clearance from the pressure side with a positive incident angle. Therefore, the heat transfer coefficient is high on the pressure side leading edge. Another area of high heat transfer coefficient occurs near the trailing section where a strong leakage inflow is induced by the pressure gradients between the pressure side and suction sides of the rotor blade. For the design condition, the tip leakage velocity enters the tip gap from the leading edge. Comparing to the low rpm case, the heat transfer coefficient increases at the leading edge while a reduction of heat transfer is observed on the trailing portion. When the rotating speed is further increased to the high rpm condition, the mainstream flow enters the clearance from the suction side with a negative incident angle. This leads to further increase of heat transfer coefficient around the lead-

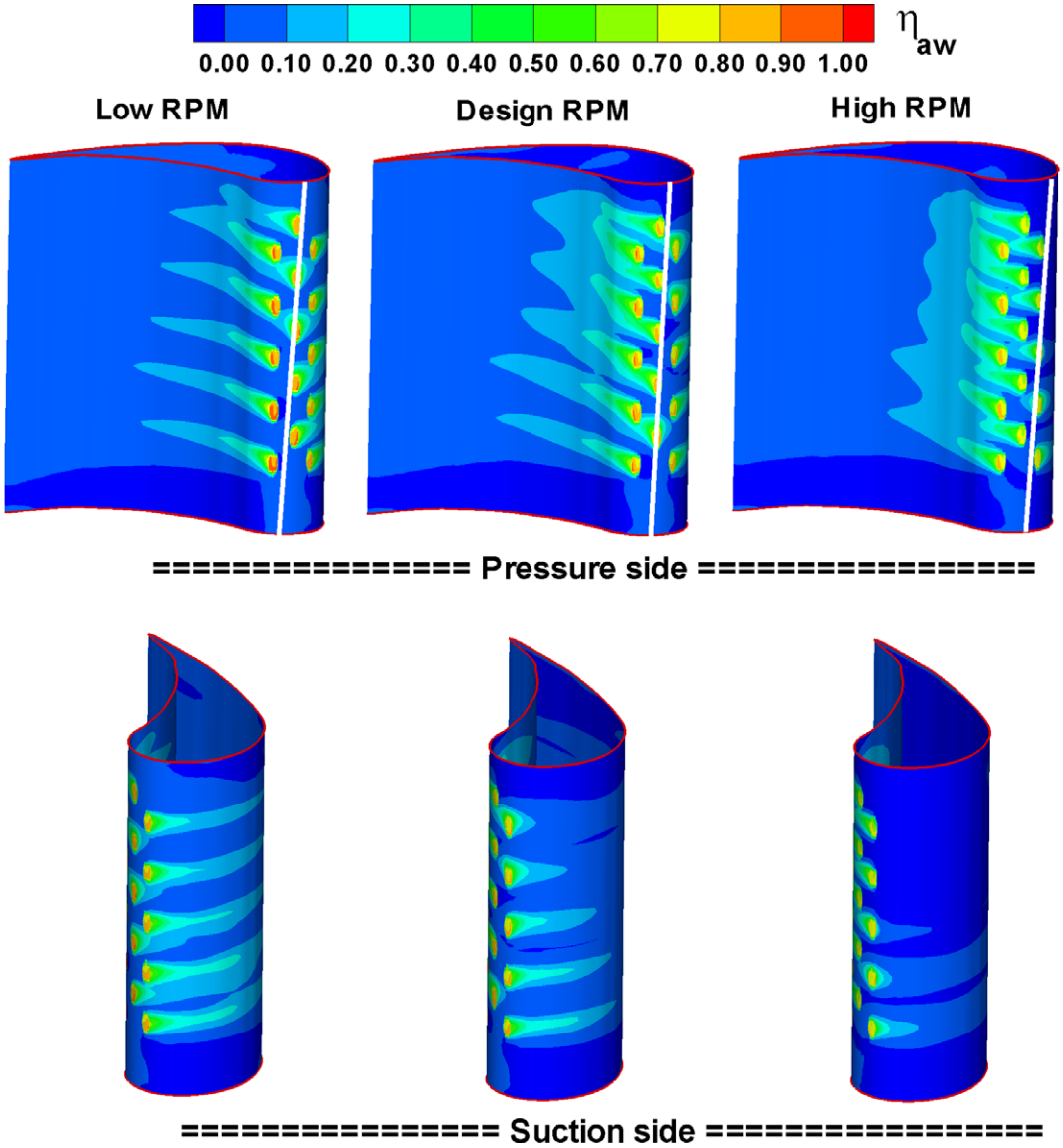

Fig. 14. Comparison of adiabatic film cooling effectiveness on the rotor and the tilted stagnation lines for various rotating speeds at time phase 1/4 and $M = 1$.

ing edge and a significant reduction of the heat transfer on the trailing portion. The general trend of the rotating effects on rotor tip heat transfer agrees well with the experiment of Rhee and Cho [10,11].

Fig. 12 compares the heat transfer coefficient on the shroud for various rotating speeds. The arrows show the incident angle of the rotor inlet relative velocity. In general, the heat transfer pattern on the shroud matches the corresponding distribution on the rotor tip for the relatively narrow tip clearance considered in the present study. The high rpm increases the shroud heat transfer coefficient in the area directly opposite to the rotor leading portion suction side, and reduces the heat transfer on the shroud surface opposite to the tip trailing portion. The effects of tip leakage vortex can also be seen from the low heat transfer strips on the shroud, which developed along the rotor suction side trailing portion. A detailed examination of the heat transfer patterns shown in Figs. 11 and 12 clearly indicates that the high rotating speed reduces tip leakage flow and shifts it to the trailing section of the rotor blade.

5. Film cooling effectiveness study

Fig. 13 compares the adiabatic film cooling effectiveness on the rotor at various time phases under the design condition at $M = 1$. As expected, the coolant jet evenly splits on both the pressure and suction sides with the stagnation line located on the leading edge. In general, the stator–rotor interaction may be attributed to several factors including: (1) the pressure field induced by the moving rotor propagates to the upstream and downstream stators; (2) the wake of the first-stage stator impinges on different parts of the rotor at different time phases; and (3) the shock wave in transonic and supersonic flow conditions. For the subsonic flow considered in the present study, the effect of shock is absent. It is seen from Fig. 13 that the film cooling effectiveness varies significantly among four different time phases due to stator–rotor interactions. A more detailed study of the unsteady characteristics of film cooling effectiveness and heat transfer coefficients was given in Yang et al. [22] for the present 1-1/2 turbine stage.

Fig. 14 shows the adiabatic film cooling effectiveness on the rotor blade surface for various rotating speeds at overall blowing ratio $M = 1$. For the low rpm condition, the stagnation line lies on the leading edge pressure side, and tilted from the pressure side root region to the suction side tip region. Therefore, most of the leading edge row and suction side row coolant shifts to the suction side, while pressure side row coolant remains on the pressure side. The top region leading edge row coolant shifts to the pressure side because of the tilted stagnation line. For the design condition, the tilted stagnation line moves to the leading edge. Consequently, the coolant splits fairly evenly on both the pressure and suction sides of the rotor blade. For the high rpm case, the tilted stagnation line moves to the suction side so most of the coolant jets shift to the pressure side except for the bottom two suction side row coolant jets which continue to protect the blade suction side.

Fig. 15 compares the predicted film cooling effectiveness with the PSP measurement by Ahn et al. [23] on the rotor leading region for $M = 1$ under various rotating speeds. It should be noted that the PSP experiments were conducted at 2400, 2550, and 3000 rpm for the low, design, and high rpm working conditions, respectively. However, the present calculations were performed at 2100, 2550, and 3000 rpm with a wider separation between the low rpm

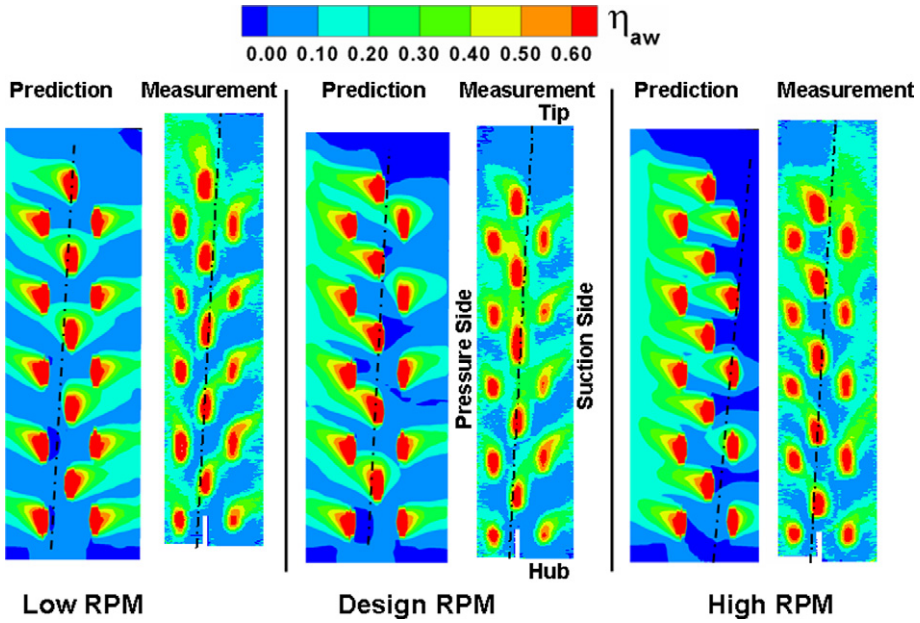

Fig. 15. Comparison of predicted and measured film cooling effectiveness distributions on the rotor leading edge for various rotating speeds at $M = 1$.

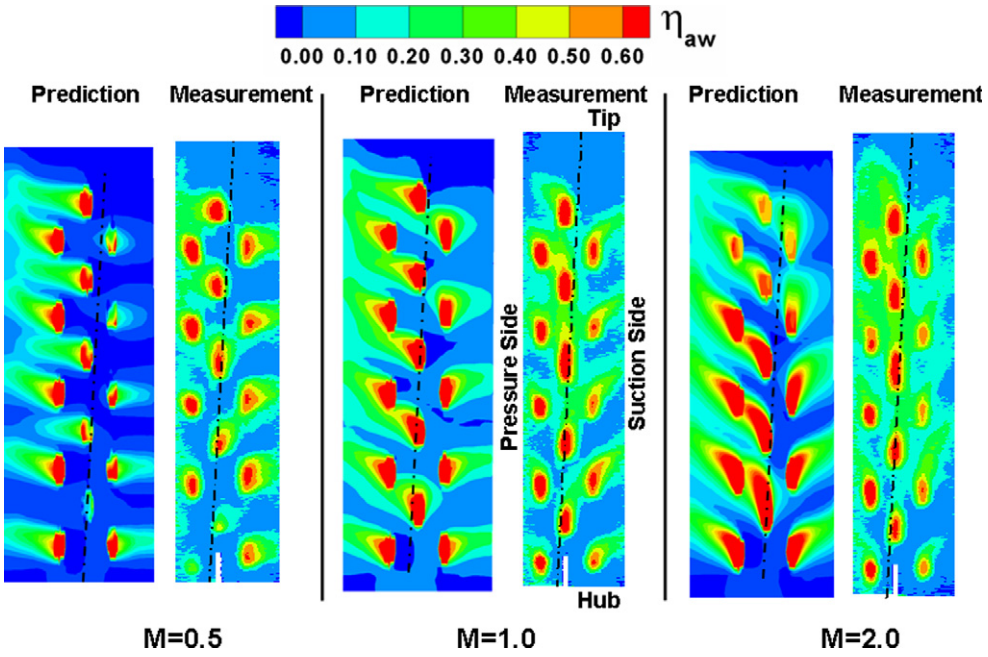

Fig. 16. Comparison of predicted and measured film cooling effectiveness distributions on the rotor leading edge for different blowing ratios at design rpm.

and design conditions. In general, the predicted film cooling patterns match well with the corresponding measurements. The stagnation line moves from pressure side to suction side with increasing rotating speed. As a result, more coolant is directed to the pressure side when M increases. The shift of the predicted film coolant traces in the blade hub and tip regions due to the tilted stagnation line are also confirmed by the experiment. The simulation, however, tends to overpredict the film cooling effectiveness and the movement of the stagnation line in comparison with the corresponding measurement.

Fig. 16 shows a comparison of the predicted and measured film cooling effectiveness for various blowing ratios at design rpm. Both prediction and experiment show that more coolant goes to the radial direction as blowing ratio increases. The lowest film cooling effectiveness was obtained at $M = 0.5$. The experiment results show a significant increase of film cooling effectiveness for $M = 1$ case, but the pattern for $M = 2$ is quite similar to the $M = 1$ case. On the other hand, the predicted film cooling effectiveness continued to increase for higher blowing ratio cases. Possible coolant jets lift-off were observed in the experiment of Ahn et al. [23] for the $M = 1$ and $M = 2$ cases. The simulation results also predicted the lift-off of coolant jets, but the film cooling effectiveness was somewhat over-predicted for the high blowing ratio cases.

6. Conclusions

Numerical simulations were performed for film cooled rotor blade with three rows of film cooling holes on the leading edge region. The heat transfer characteristics for tip leakage flow are included. The unsteady film cooling effectiveness and heat transfer coefficients on the film cooled rotor blade are investigated for both the design and off-design conditions. The primary findings from this study are summarized as follows:

1. The rotating speed is the most critical parameter in determining the heat transfer and film cooling effectiveness distributions for the leading edge film cooling. An increase in rotating speed reduces the rotor relative inlet velocity and changes the incidence angle to the leading edge of the rotor blade.
2. The stagnation line tilts from the pressure side root region to the suction side tip region for the present two-dimensional blade. With increasing rotating speed, the tilted stagnation line is shifted from the pressure side to suction side.
3. The coolant jets disturb the mainstream flow and increase the heat transfer downstream of the film holes. With increasing rotating speed, the rotor overall heat transfer decreases due to the reduced relative inlet velocity. Higher rpm significantly augments the heat transfer on the rotor tip leading edge while decreases the heat transfer on the trailing portion of rotor blade tip.
4. With increasing rotating speed, the coolant protection is shifted from the suction side to the pressure side. As the blowing ratio increases, the predicted film cooling distribution is more uniform and the averaged film cooling effectiveness increases slightly.
5. The general trend of the numerical simulations is in reasonably good agreement with the experimental data. However, the level of film cooling effectiveness is somewhat overpredicted while the coolant jets lift-off is underpredicted.

Acknowledgements

The project is partially supported by Solar Turbines Company. The authors want to thank Dr. M.T. Schobeiri at Texas A&M University for his providing the turbine rig geometry and flow conditions.

References

[1] M.G. Dunn, Heat flux measurement for a rotor of a full stage turbine. Part I: Time averaged results, ASME J. Turbomach. 108 (1) (1986) 90–97.
[2] M.G. Dunn, W.K. George, W.J. Rae, S.H. Woodward, J.C. Moller, J.P. Seymour, Heat flux measurement for a rotor of a full stage turbine. Part II: Description of analysis technique and typical time-resolved measurements, ASME J. Turbomach. 108 (1) (1986) 98–107.
[3] R.S. Abhari, A.H. Epstein, An experimental study of film cooling in a rotating transonic turbine, ASME J. Turbomach. 116 (1) (1994) 63–70.
[4] K. Takeishi, S. Aoki, T. Sato, Film cooling on a gas turbine rotor blade, ASME J. Turbomach. 114 (4) (1992) 828–834.
[5] C. Camci, T. Arts, Short-duration measurement and numerical simulation of heat transfer along the suction side of a gas turbine blade, ASME J. Eng. Gas Turbines Power 107 (4) (1985) 991–997.
[6] C. Camci, T. Arts, Experimental heat transfer investigation around the film cooled leading edge of a high pressure gas turbine rotor blade, ASME J. Eng. Gas Turbines Power 107 (4) (1985) 1016–1021.
[7] A.B. Mehendale, S.V. Ekkad, J.C. Han, Mainstream turbulence effect on film effectiveness and heat transfer coefficient of a gas turbine blade with air and CO_2 film injection, International J. Heat Mass Transfer 37 (10) (1994) 2707–2714.
[8] A.B. Mehandale, J.C. Han, S. Ou, C.P. Lee, Unsteady wake over a linear turbine blade cascade with air and CO_2 film injection. Part II: Effect on film effectiveness and heat transfer distributions, ASME J. Turbomach. 116 (4) (1994) 730–737.
[9] H. Du, J.C. Han, S.V. Ekkad, Effect of unsteady wake on detailed heat transfer coefficient and film effectiveness distribution for a gas turbine blade, ASME J. Turbomach. 120 (4) (1998) 808–817.
[10] D.H. Rhee, H.H. Cho, Local transfer characteristics on a rotating blade with flat tip in a low speed annular cascade: Part 1 – near-tip surface, ASME paper GT2005-68723.
[11] D.H. Rhee, H.H. Cho, Local heat/mass transfer characteristics on a rotating blade with flat tip in a low speed annular cascade: Part 2 – tip and shroud, ASME paper GT2005-68724.
[12] J. Ahn, M.T. Schobeiri, J.C. Han, H.K. Moon, Film cooling effectiveness on the leading edge of a rotating turbine blade, ASME Paper IMECE 2004-59852.
[13] R.S. Abhari, G.R. Guenette, A.H. Epstein, M.B. Giles, Comparison of time-resolved turbine rotor blade heat transfer measurements and numerical calculations, in: ASME International Gas Turbine & Aeroengine Congress & Exposition, Orlando, FL, ASME Paper 91-GT-268, June1991.
[14] M.G. Dunn, J. Kim, K.C. Givinkas, R.J. Boyle, Time averaged heat transfer and pressure measurement and comparison with prediction for a two-stage turbine, in: ASME International Gas Turbine & Aeroengine Congress & Exposition, Cologine, Germany, ASME Paper 92-GT-194, June 1992.
[15] A.A. Ameri, E. Steinthorsson, Prediction of unshrouded rotor blade tip heat transfer, in: ASME International Gas Turbine & Aeroengine Congress & Exposition, Houston, TX, ASME Paper 95-GT-189, June 1995.
[16] Q. Zhang, P.M. Ligrani, Numerical predictions of Stanton numbers, skin friction coefficients, aerodynamic losses, and Reynolds analogy behavior for a transonic turbine vane, Numer. Heat Transfer Part A 49 (2006) 237–256.
[17] Y.L. Lin, M.A. Stephens, T.I-P. Shih, Computation of leading edge film cooling with injection through rows of compound angel holes, in: ASME International Gas Turbine & Aeroengine Congress & Exhibition, Orlando, FL, ASME Paper 97-GT-298, June 1997.
[18] V.K. Garg, A.A. Ameri, Comparison of two-equation turbulence models for prediction of heat transfer on film-cooled turbine blades, Numer. Heat Transfer Part A 32 (4) (1997) 347–355.
[19] H. Yang, S. Acharya, S.V. Ekkad, C. Prakash, R. Bunker, Flow and heat transfer prediction for a flat-tip turbine blade, ASME Paper, GT-2002-30190.
[20] H. Yang, S. Acharya, S.V. Ekkad, C. Prakash, R. Bunker, Numerical simulation of flow and heat transfer past a turbine blade with a squealer tip, ASME Paper GT-2002-30193.
[21] H. Yang, H.C. Chen, J.C. Han, Film-cooling prediction on turbine blade tip with various film hole configurations, AIAA J. Thermophys. Heat Transfer 20 (3) (2006) 558–568.
[22] H. Yang, H.C. Chen, J.C. Han, Numerical prediction of film cooling and heat transfer on the leading edge of a rotating blade in a 1-1/2 turbine stage, ASME Paper IMECE 2004-59599.
[23] J. Ahn, M.T. Schobeiri, J.C. Han, H.K. Moon, Effect of rotation on leading edge region film cooling of a gas turbine blade with three rows of film cooling holes, Int. J. Heat Mass Transfer 50 (2007) 15–25.
[24] M.T. Schobeiri, A. Suryanarayanan, C. Jermann, T. Neuenschwander, A comparative aerodynamic and performance study of a three-stage high pressure turbine with 3-d bowed blades and cylindrical blades, ASME Paper GT2004-53650.
[25] M.T. Schobeiri, J.L Gilarranz, E.S. Johansen, Aerodynamic and performance studies of a three stage high pressure research turbine with 3-D blades, design points and off-design experimental investigations, ASME Paper 2000-GT-484.
[26] Fluent Inc., Fluent User's Guide in CD-ROM, Version 6.0, Fluent Inc. New Hampshire.
[27] H. Yang, H.C. Chen, J.C. Han, Numerical study of a rotating blade platform with film cooling from cavity purge flow in a 1-1/2 turbine stage, ASME paper GT2006-90322.